

Measurement of the Three-Flavor Composition of Astrophysical Neutrinos with Contained IceCube Events

The IceCube Collaboration

(a complete list of authors can be found at the end of the proceedings)

E-mail: abalagopalv@icecube.wisc.edu, vbasu@icecube.wisc.edu,
karle@icecube.wisc.edu

The IceCube Neutrino Observatory at the South Pole detects neutrinos from the entire sky, both of astrophysical and atmospheric origin, via the Cherenkov light emitted when these neutrinos interact in the ice, giving rise to rapidly moving charged particles. Neutrino events with vertices contained within the detector volume are useful for studying the neutrino flavor ratio, as they allow for a better reconstruction of the event morphology. The Medium Energy Starting Events (MESE) data sample is a selection of such events with energies of at least 1 TeV. This sample includes electron-, muon-, and tau-neutrino events, processed consistently. We use it to constrain the flavor ratio of astrophysical neutrinos at Earth, which in turn informs us of the flavor composition at the source itself. In this talk, we will present the results of this study, based on 11.4 years of IceCube data.

Corresponding authors: Aswathi Balagopal V.^{1*}, Vedant Basu², Albrecht Karle³

¹ *University of Delaware*

² *University of Utah*

³ *University of Wisconsin-Madison*

* Presenter

39th International Cosmic Ray Conference (ICRC2025)
15–24 July 2025
Geneva, Switzerland



1. Introduction

The IceCube Neutrino Observatory, located at the South Pole, detects neutrinos via the Cherenkov light deposited by their charged secondaries produced as they interact in ice [1]. These can be charged current (CC) or neutral current (NC) interactions of electron, muon, or tau neutrinos. The Cherenkov light produced by the secondaries is detected using 5160 digital optical modules (DOMs) hosted on 86 strings inserted into the glacier. The detector measures signal from neutrinos of atmospheric and astrophysical origin with energies of hundreds of GeV and above. Muons generated from cosmic-ray air showers are also seen in the detector, and constitute the major background for astrophysical neutrino detection.

Here we use a selection of events called 'Medium Energy Starting Events' (MESE) [2], with a total of 9888 events with interaction vertices inside the detector ("starting events") and with energies of 1 TeV and above. The selection is based on a series of veto criteria to reject muon events to obtain a neutrino-rich dataset. The MESE sample consists of electron, muon and tau neutrinos from the whole sky. Based on the distribution of light in the detector, the morphology of the observed events can be classified into cascades, tracks, and double cascades. Cascades arise from CC interactions of electron neutrinos and NC interactions of all neutrino flavors. Tracks are produced in CC interactions of muon neutrinos or tau neutrinos where the tau lepton decays into muons while other CC interactions of tau neutrinos produce double cascades. The MESE sample is also used for measuring the cosmic neutrino spectrum, as described in [3]. The sample used here has a few additional events compared to that used in [3] since an additional cut on the required number of active DOMs is implemented in [3] and not here.

Since the MESE sample has neutrinos of all flavors, it is suitable for measuring the astrophysical flavor ratio of neutrinos. Cascades and tracks within the dataset are classified as such during the selection procedure, using a deep neural network [4], with $\sim 88\%$ efficiency for true cascades and $\sim 97\%$ for true tracks above 1 TeV. A majority of the true double cascade events in the sample are classified as single cascades by the deep neural network, which makes it difficult to break the degeneracy between electron and tau neutrinos while measuring the flavor ratio. We therefore introduce an additional classification strategy in this analysis, designed specifically to select double cascade events.

2. Method

The double-cascade selection method is likelihood-based and similar to that described in [5]. Final-level events in the MESE sample, that are already classified as either cascades or tracks, are passed through a reconstruction algorithm that maximizes the likelihood under a double-cascades hypothesis, using the spatial and timing information of the deposited charge in the DOMs. Several variables are extracted from the event based on these reconstructions: the energy of each cascade in the double-cascade event, the sum of the energies of the two cascades, the sum of the energies deposited within 40 m of each cascade vertex compared to the total energy, the relative energy asymmetry between the two cascades, and the decay length of the tau lepton obtained from the separation between the two cascades. Events that fall within a given range for these observables, predefined using simulations of neutrinos of all flavors, are retained for the double

cascade classification [5]. The final list of events accepted into the double cascade classification are events that pass these conditions, and have a reconstructed total energy greater than 30 TeV and reconstructed length greater than 10 meters to prevent misclassification from a majority of the background. These restrictions result in an expected number of 7 events, with 70% purity. The remaining events retain their original classification as cascades or tracks. The low count of double-cascade events is attributed to the difficulty in separating them out due to the spacing of the DOMs in the detector. A majority of tau neutrinos in the sample have energies on the TeV scale, due to the falling nature of the flux, and therefore have tau decay lengths in the scale of a few meters to a few tens of meters. This makes the separation between the two cascades difficult as the spacing between the strings holding the DOMs is ~ 125 meters.

We use observables from these classified events, both from data and simulations, to perform a forward-folded fit and measure the astrophysical flavor ratio. We generate 2D histograms of reconstructed energy vs. cosine of the reconstructed zenith angle for cascades and tracks. Double cascades are additionally also binned according to the reconstructed length, to form 3D histograms. The forward-folded fit includes components that account for the conventional neutrino flux arising from pion and kaon decays in cosmic ray air showers, prompt neutrino flux from charmed decays in air showers, atmospheric muon flux, and the astrophysical neutrino flux.

We assume a broken power law (BPL) as the baseline shape of the astrophysical flux, following the best-fit measurement of the spectral shape using the MESE sample [3]. Other IceCube measurements [6] also indicate a possible break in the spectrum of cosmic neutrinos. The physics parameters of the analysis reported here are the flavor ratios. We fit for the fraction of electron and tau neutrinos in the total astrophysical neutrino flux, and constrain the fraction of muon neutrinos via the relation $f_e + f_\tau + f_\mu = 1$. Systematic uncertainties in the atmospheric neutrino flux arising from uncertainties in the cosmic ray flux and the corresponding production of neutrinos are included as nuisance parameters in the fit. We also account for detector-related systematic uncertainties as nuisance parameters in the fit. These parameters allow for changes in the detector's light acceptance resulting from uncertainties in the ice model and the optical efficiency of the DOMs. Along with the baseline BPL fit, we also fit for a single power law (SPL) astrophysical flux assumption as a cross-check, since previous IceCube measurements were consistent with an SPL shape for the astrophysical flux. This fit is performed under the assumption that the flavor ratio remains the same across the energy scales considered here i.e. 1 TeV to 10 PeV. We use the software package NNMFIT to perform the fit [7].

3. Results

The number of events in the MESE sample used for the flavor measurement with 11.4 years of IceCube data is shown in Table 1. This is compared to the expected number of events from the best-fit to the BPL and SPL models.

The energy distributions of cascades, tracks, and double cascades are shown in Figure 1. Observed data is compared to the total MC, under our best-fit BPL spectrum with normalization $\phi = 2.72^{+0.95}_{-0.92} \times 10^{-18} \text{ GeV/cm}^2/\text{s/sr}$, the lower energy spectral index $\gamma_1 = 1.76^{+0.36}_{-0.26}$, the higher energy index $\gamma_2 = 2.81^{+0.08}_{-0.12}$ and the break energy $\log_{10}(E_{\text{break}}/\text{GeV}) = 4.5^{+0.12}_{-0.09}$. The best fit astrophysical flavor ratio at Earth is obtained as $f_e : f_\mu : f_\tau = 0.30 : 0.37 : 0.33$. The figure shows

Morphology	Data	BPL	SPL
Cascades	4960	4953.6 ± 154.6	4999.2 ± 160.4
Tracks	4919	4876.2 ± 136.1	4825.4 ± 141.7
Double Cascades	9	7.0 ± 0.9	9.1 ± 1.0

Table 1: Number of cascades ($E > 1$ TeV), tracks ($E > 1$ TeV), and double cascades ($E > 30$ TeV) in data compared to expectation from best-fit to BPL and SPL models. Both statistical and systematic uncertainties are included in the reported errors.

that data and the best-fit MC are compatible with each other within 2σ . This is also the case for the other observables used in the fit: cosine of reconstructed zenith (for all three morphologies) and reconstructed length (for double cascades). Since only 9 double-cascade classified events exist in data, consistent with the expectation from MC, we have large statistical uncertainties in the double cascades histograms.

Figure 2 shows the 68% and 95% Wilks' contours obtained from the fit on a ternary diagram showing the fraction of each neutrino flavor on Earth. Also shown in the figure are the expectations for several flavor assumptions at source, after averaged oscillations during their journey from the source to the Earth. These source assumptions are: pion decay resulting in a flavor ratio of 1:2:0 at source, muon damped pion decay with a ratio of 0:1:0, and neutron decay with a ratio of 1:0:0. The best fit is seen to be consistent with expectations from the standard theory of neutrino oscillations, as any deviation from this would result in the best fit lying in a region that is not along the line connecting the three standard source scenarios shown in the figure.

The figure also shows the best fit and the Wilks' contours under the SPL assumption. While the best fits and the shape of the contours with the BPL and SPL fits remain comparable, it is seen that the 95% CL contour closes under the SPL assumption and does not under the BPL assumption. The reason for this is the harder spectral index ($\gamma = 2.54^{+0.05}_{-0.04}$) fitted for the SPL model, resulting in a prediction of a larger number of high-energy neutrinos and, therefore, a larger fraction of events with longer tau decay-lengths, recognizable as double-cascades. This results in the inability to close the 95% contour for the BPL model. This also demonstrates the necessity to model the spectrum properly to obtain an accurate measurement of the flavor ratio.

Figure 3 shows the measurement of the flavor ratio in this analysis compared to previous measurements from IceCube. We can see that the 68% CL contour closes for the first time with this analysis, marking a milestone in IceCube's measurements of the astrophysical flavor ratio. This can be attributed to the following:

- Inclusion of tau-neutrino classification: This breaks the degeneracy between electron and tau neutrinos. For example, 'Combined Fit (2015)' [8] and 'Inelasticity (2019)' [9] in the figure did not include any classification of tau neutrino based morphologies. This makes it difficult to close the contours either along the ν_e or ν_τ axis.
- Inclusion of TeV-scale events: This increases the total number of events, especially for the cascade and track morphologies when compared to using only the high energy events (above 60 TeV) as done in 'HESE (2022)' [5]. This in turn, gives strong constraints from

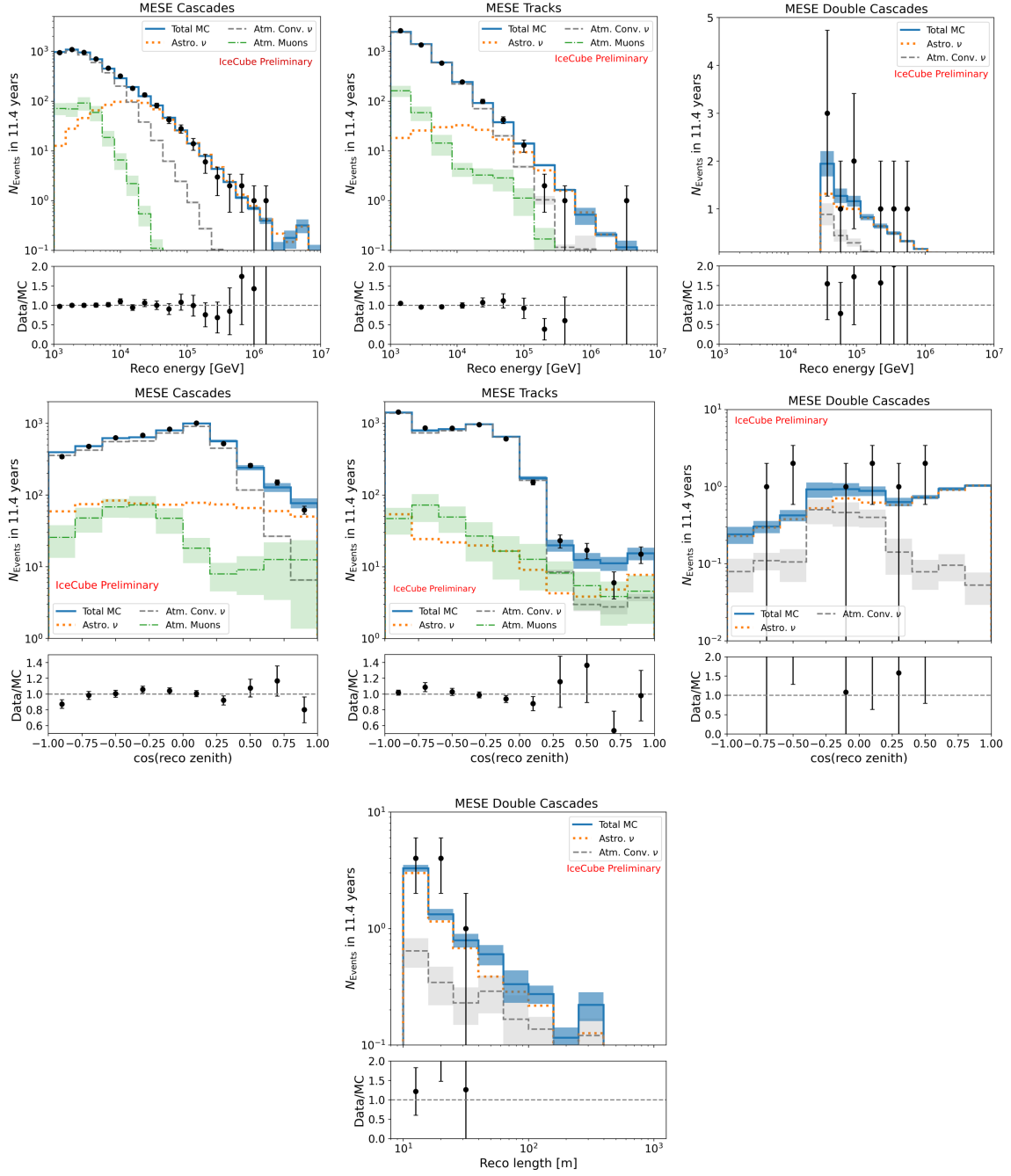


Figure 1: The 1D projections of the reconstructed energy and reconstructed cosine zenith distributions of cascade, track, and double cascade classified events in MESE. The reconstructed length distribution for double cascade classified events is also shown. Data is shown in black and total best-fit MC is shown in blue. The individual components of the total MC are also shown in the figure. The prompt atmospheric flux fits to zero and is therefore not shown in the figure. No atmospheric muons pass the double-cascade classification.

higher statistics, especially along the electron and muon neutrino axes along with improved constraints on the nuisance parameters in the fit.

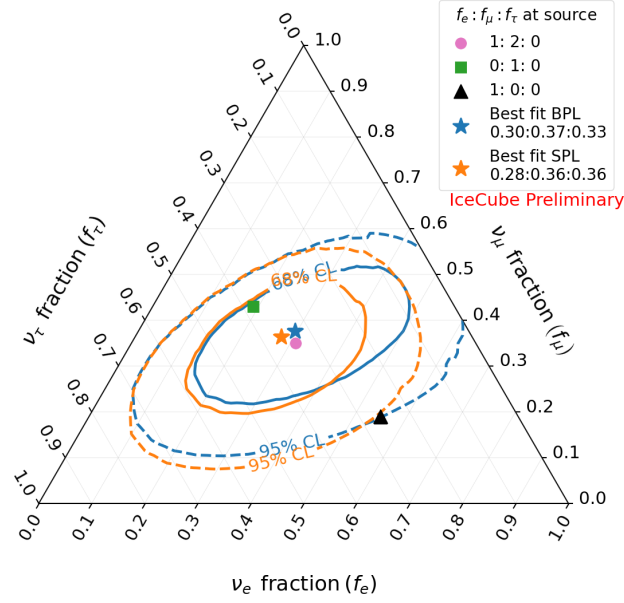


Figure 2: Fits to the astrophysical flavor ratio with the MESE sample for the baseline assumption of a BPL flux (blue) and for the cross-check with an SPL fit (orange). 68% CL and 95% CL Wilks' contours are shown here along with the best fit. The best fit from both flux assumptions are consistent with each other. Assumptions of flavor ratio at source, after undergoing oscillations during their propagation towards Earth are also shown in the figure.

- An increased livetime: We use 11.4 years of data collected with IceCube in this analysis.

4. Conclusion

The results presented here show that, for the first time, we are able to constrain the fraction of neutrinos of each flavor of neutrino to be > 0 with more than 68% CL. Based on the maximum-likelihood test, we reject zero electron neutrinos with 98.7% CL and a zero fraction of tau neutrinos with 91.9% CL. While the best fit flavor ratio of $f_e : f_\mu : f_\tau = 0.30 : 0.37 : 0.33$ is closest to the standard pion decay scenario, the muon-damped source scenario is still within the 68% CL contour. A neutrino flux dominated by neutron decay at source is rejected at 94.8% CL with the Wilks' contour from the maximum-likelihood fit. Although a previous analysis from IceCube ('Combined Fit (2015)' [8]) rejected the neutron-decay scenario at a higher confidence level, the previous analysis used no information about tau neutrinos. This analysis uses an updated treatment of systematics and better modeling of the ice, which affects light propagation and therefore the description of signal collection by the DOMs. The best fit of the flavor ratio lies on the line connecting the three standard source scenarios, which is the only region allowed by the standard theory of neutrino oscillations [10]. Therefore, our results are consistent with this theory. Future studies including other methods of classifying tau-neutrino events, for instance a neural-network

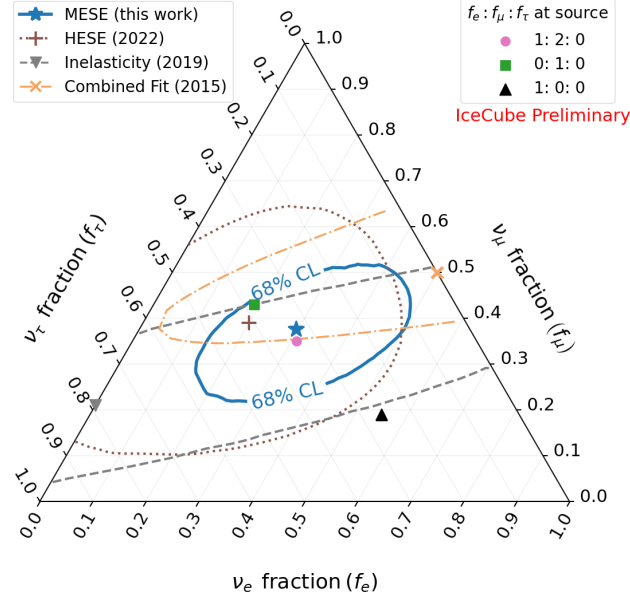


Figure 3: A comparison of the flavor ratio measured with the MESE sample to previous measurements made with IceCube [8] [9] [5] is shown. All curves show the 68% CL Wilks' contours, along with the respective best fit. Previous measurements with IceCube assumed an SPL flux when measuring the flavor ratio, while this work assumes the flux to be a BPL, consistent with IceCube's latest spectral measurements [3]. Including the double-cascades classification along with the cascades and tracks classification helps the contour close in the MESE analysis.

based classification [11] or identification of tracks induced by tau neutrinos [9, 12] can be expected to provide a larger sample of tau neutrino classified events to be included in the flavor measurement.

References

- [1] **IceCube** Collaboration, M. G. Aartsen *et al.*, *JINST* **12** no. 03, (2017) P03012.
- [2] **IceCube** Collaboration, V. Basu and A. Balagopal V., *PoS (ICRC2023)* 1007.
- [3] **IceCube** Collaboration, *PoS ICRC2025* (these proceedings) 985.
- [4] **IceCube** Collaboration, M. Kronmueller and T. Glauch, *PoS (ICRC2019)* 937.
- [5] **IceCube** Collaboration, R. Abbasi *et al.*, *Eur. Phys. J. C* **82** no. 11, (2022) 1031.
- [6] **IceCube** Collaboration, R. Naab, E. Ganster, and Z. Zhang, *PoS (ICRC2023)* 1064.
- [7] C. Haack, E. Ganster, *et al.*, “NNMFit - an aesara-based analysis framework for diffuse analyses.” paper in preparation.
- [8] **IceCube** Collaboration, M. G. Aartsen *et al.*, *Astrophys. J.* **809** no. 1, (2015) 98.

- [9] **IceCube** Collaboration, M. G. Aartsen *et al.*, *Phys. Rev. D* **99** no. 3, (2019) 032004.
- [10] N. Song, S. W. Li, C. A. Argüelles, M. Bustamante, and A. C. Vincent, *JCAP* **04** (2021) 054.
- [11] **IceCube** Collaboration, R. Abbasi *et al.*, *Phys. Rev. Lett.* **132** no. 15, (2024) 151001.
- [12] R. Clark, *Measuring high energy diffuse fluxes at the South Pole with the IceCube Neutrino Observatory and DM-Ice17*. PhD thesis, 2025.

Full Author List: IceCube Collaboration

R. Abbasi¹⁶, M. Ackermann⁶³, J. Adams¹⁷, S. K. Agarwalla^{39, a}, J. A. Aguilar¹⁰, M. Ahlers²¹, J.M. Alameddine²², S. Ali³⁵, N. M. Amin⁴³, K. Andeen⁴¹, C. Argüelles¹³, Y. Ashida⁵², S. Athanasiadou⁶³, S. N. Axani⁴³, R. Babu²³, X. Bai⁴⁹, J. Baines-Holmes³⁹, A. Balagopal V.^{39, 43}, S. W. Barwick²⁹, S. Bash²⁶, V. Basu⁵², R. Bay⁶, J. J. Beatty^{19, 20}, J. Becker Tjus^{9, b}, P. Behrens¹, J. Beise⁶¹, C. Bellenghi²⁶, B. Benkel⁶³, S. BenZvi⁵¹, D. Berley¹⁸, E. Bernardini^{47, c}, D. Z. Besson³⁵, E. Blaufuss¹⁸, L. Bloom⁵⁸, S. Blot⁶³, I. Bodo³⁹, F. Bontempo³⁰, J. Y. Book Motzkin¹³, C. Boscolo Meneguolo^{47, c}, S. Böser⁴⁰, O. Botner⁶¹, J. Böttcher¹, J. Braun³⁹, B. Brinson⁴, Z. Brisson-Tsavoussis³², R. T. Burley², D. Butterfield³⁹, M. A. Campana⁴⁸, K. Carloni¹³, J. Carpio^{33, 34}, S. Chattopadhyay^{39, a}, N. Chau¹⁰, Z. Chen⁵⁵, D. Chirkin³⁹, S. Choi⁵², B. A. Clark¹⁸, A. Coleman⁶¹, P. Coleman¹, G. H. Collin¹⁴, D. A. Coloma Borja⁴⁷, A. Connolly^{19, 20}, J. M. Conrad¹⁴, R. Corley⁵², D. F. Cowen^{59, 60}, C. De Clercq¹¹, J. J. DeLaunay⁵⁹, D. Delgado¹³, T. Delmeulle¹⁰, S. Deng¹, P. Desiati³⁹, K. D. de Vries¹¹, G. de Wasseige³⁶, T. DeYoung²³, J. C. Díaz-Vélez³⁹, S. DiKerby²³, M. Dittmer⁴², A. Domi²⁵, L. Draper⁵², L. Dueser¹, D. Durnford²⁴, K. Dutta⁴⁰, M. A. DuVernois³⁹, T. Ehrhardt⁴⁰, L. Eidenschink²⁶, A. Eimer²⁵, P. Eller²⁶, E. Ellinger⁶², D. Elsässer²², R. Engel^{30, 31}, H. Erpenbeck³⁹, W. Esmail⁴², S. Eulig¹³, J. Evans¹⁸, P. A. Evenson⁴³, K. L. Fan¹⁸, K. Fang³⁹, K. Farrag¹⁵, A. R. Fazely⁵, A. Fedynitch⁵⁷, N. Feigl⁸, C. Finley⁵⁴, L. Fischer⁶³, D. Fox⁵⁹, A. Franckowiak⁹, S. Fukami⁶³, P. Fürst¹, J. Gallagher³⁸, E. Ganster¹, A. Garcia¹³, M. Garcia⁴³, G. Garg^{39, a}, E. Genton^{13, 36}, L. Gerhardt⁷, A. Ghadimi⁵⁸, C. Glaser⁶¹, T. Glüsenskamp⁶¹, J. G. Gonzalez⁴³, S. Goswami^{33, 34}, A. Granados²³, D. Grant¹², S. J. Gray¹⁸, S. Griffin³⁹, S. Griswold⁵¹, K. M. Groth²¹, D. Guevel³⁹, C. Günther¹, P. Gutjahr²², C. Ha⁵³, C. Haack²⁵, A. Hallgren⁶¹, L. Halve¹, F. Halzen³⁹, L. Hamacher¹, M. Ha Minh²⁶, M. Handt¹, K. Hanson³⁹, J. Hardin¹⁴, A. A. Harnisch²³, P. Hatch³², A. Haungs³⁰, J. Häußler¹, K. Helbing⁶², J. Hellrung⁹, B. Henke²³, L. Hennig²⁵, F. Henningsen¹², L. Heuermann¹, R. Hewett¹⁷, N. Heyer⁶¹, S. Hickford⁶², A. Hidvegi⁵⁴, C. Hill¹⁵, G. C. Hill², R. Hmaid¹⁵, K. D. Hoffman¹⁸, D. Hooper³⁹, S. Hori³⁹, K. Hoshina^{39, d}, M. Hostert¹³, W. Hou³⁰, T. Huber³⁰, K. Hultqvist⁵⁴, K. Hymon^{22, 57}, A. Ishihara¹⁵, W. Iwakiri¹⁵, M. Jacquart²¹, S. Jain³⁹, O. Janik²⁵, M. Jansson³⁶, M. Jeong⁵², M. Jin¹³, N. Kamp¹³, D. Kang³⁰, W. Kang⁴⁸, X. Kang⁴⁸, A. Kappes⁴², L. Kardum²², T. Karg⁶³, M. Karl²⁶, A. Karle³⁹, A. Katil²⁴, M. Kauer³⁹, J. L. Kelley³⁹, M. Khanal⁵², A. Khatee Zathul³⁹, A. Kheirandish^{33, 34}, H. Kimku⁵³, J. Kiryluk⁵⁵, C. Klein²⁵, S. R. Klein^{6, 7}, Y. Kobayashi¹⁵, A. Kochocki²³, R. Koirala⁴³, H. Kolanoski⁸, T. Kontrimas²⁶, L. Köpke⁴⁰, C. Kopper²⁵, D. J. Koskinen²¹, P. Koundal⁴³, M. Kowalski^{8, 63}, T. Kozynets²¹, N. Krieger⁹, J. Krishnamoorthi^{39, a}, T. Krishnan¹³, K. Kruiswijk³⁶, E. Krupczak²³, A. Kumar⁶³, E. Kun⁹, N. Kurahashi⁴⁸, N. Lad⁶³, C. Lagunas Gualda²⁶, L. Lallement Arnaud¹⁰, M. Lamoureux³⁶, M. J. Larson¹⁸, F. Lauber⁶², J. P. Lazar³⁶, K. Leonard DeHolton⁶⁰, A. Leszczyńska⁴³, J. Liao⁴, C. Lin⁴³, Y. T. Liu⁶⁰, M. Liubarska²⁴, C. Love⁴⁸, L. Lu³⁹, F. Lucarelli²⁷, W. Luszczak^{19, 20}, Y. Lyu^{6, 7}, J. Madsen³⁹, E. Magnus¹¹, K. B. M. Mahn²³, Y. Makino³⁹, E. Manao²⁶, S. Mancina^{47, e}, A. Mand³⁹, I. C. Mariş¹⁰, S. Marka⁴⁵, Z. Marka⁴⁵, L. Marten¹, I. Martinez-Soler¹³, R. Maruyama⁴⁴, J. Mauro³⁶, F. Mayhew²³, F. McNally³⁷, J. V. Mead²¹, K. Meagher³⁹, S. Mechbal⁶³, A. Medina²⁰, M. Meier¹⁵, Y. Merckx¹¹, L. Merten⁹, J. Mitchell⁵, L. Molchany⁴⁹, T. Montaruli²⁷, R. W. Moore²⁴, Y. Morii¹⁵, A. Mosbrugger²⁵, M. Moulai³⁹, D. Mousadi⁶³, E. Moyaux³⁶, T. Mukherjee³⁰, R. Naab⁶³, M. Nakos³⁹, U. Naumann⁶², J. Necker⁶³, L. Neste⁵⁴, M. Neumann⁴², H. Niederhausen²³, M. U. Nisa²³, K. Noda¹⁵, A. Noell¹, A. Novikov⁴³, A. Obertacke Pollmann¹⁵, V. O'Dell³⁹, A. Olivas¹⁸, R. Orsoe²⁶, J. Osborn³⁹, E. O'Sullivan⁶¹, V. Palusova⁴⁰, H. Pandya⁴³, A. Parenti¹⁰, N. Park³², V. Parrish²³, E. N. Paudel⁵⁸, L. Paul⁴⁹, C. Pérez de los Heros⁶¹, T. Pernice⁶³, J. Peterson³⁹, M. Plum⁴⁹, A. Pontén⁶¹, V. Poojyam⁵⁸, Y. Popovych⁴⁰, M. Prado Rodriguez³⁹, B. Pries²³, R. Procter-Murphy¹⁸, G. T. Przybylski⁷, L. Pyras⁵², C. Raab³⁶, J. Rack-Helleis⁴⁰, N. Rad⁶³, M. Ravn⁶¹, K. Rawlins³, Z. Rechav³⁹, A. Rehman⁴³, I. Reistoffer⁴⁹, E. Resconi²⁶, S. Reusch⁶³, C. D. Rho⁵⁶, W. Rhode²², L. Ricca³⁶, B. Riedel³⁹, A. Rifaie⁶², E. J. Roberts², S. Robertson^{6, 7}, M. Rongen²⁵, A. Rosted¹⁵, C. Rott⁵², T. Ruhe²², L. Ruohan²⁶, D. Ryckbosch²⁸, J. Saffer³¹, D. Salazar-Gallegos²³, P. Sampathkumar³⁰, A. Sandrock⁶², G. Sanger-Johnson²³, M. Santander⁵⁸, S. Sarkar⁴⁶, J. Savelberg¹, M. Scarnera³⁶, P. Schaile²⁶, M. Schaufel¹, H. Schieler³⁰, S. Schindler²⁵, L. Schlickmann⁴⁰, B. Schlüter⁴², F. Schlüter¹⁰, N. Schmeisser⁶², T. Schmidt¹⁸, F. G. Schröder^{30, 43}, L. Schumacher²⁵, S. Schwirn¹, S. Sclafani¹⁸, D. Seckel⁴³, L. Seen³⁹, M. Seikh³⁵, S. Seunarine⁵⁰, P. A. Seville Myhr³⁶, R. Shah⁴⁸, S. Shefali³¹, N. Shimizu¹⁵, B. Skrzypek⁶, R. Snihur³⁹, J. Soedingrekso²², A. Sogaard²¹, D. Soldin⁵², P. Soldin¹, G. Sommani⁹, C. Spannfellner²⁶, G. M. Spiczak⁵⁰, C. Spiering⁶³, J. Stachurska²⁸, M. Stamatikos²⁰, T. Stanev⁴³, T. Stezelberger⁷, T. Stürwald⁶², T. Stüttard²¹, G. W. Sullivan¹⁸, I. Taboada⁴, S. Ter-Antonyan⁵, A. Terliuk²⁶, A. Thakuri⁴⁹, M. Thiesmeyer³⁹, W. G. Thompson¹³, J. Thwaites³⁹, S. Tilav⁴³, K. Tollefson²³, S. Toscano¹⁰, D. Tosi³⁹, A. Trettin⁶³, A. K. Upadhyay^{39, a}, K. Upshaw⁵, A. Vaidyanathan⁴¹, N. Valtonen-Mattila^{9, 61}, J. Valverde⁴¹, J. Vandenbroucke³⁹, T. van Eeden⁶³, N. van Eijndhoven¹¹, L. van Rootselaar²², J. van Santen⁶³, F. J. Vara Carbonell⁴², F. Varsi³¹, M. Venugopal³⁰, M. Vereecken³⁶, S. Vergara Carrasco¹⁷, S. Verpoest⁴³, D. Veske⁴⁵, A. Vijai¹⁸, J. Villarreal¹⁴, C. Walck⁵⁴, A. Wang⁴, E. Warrick⁵⁸, C. Weaver²³, P. Weigel¹⁴, A. Weindl³⁰, J. Weldert⁴⁰, A. Y. Wen¹³, C. Wendt³⁹, J. Werthebach²², M. Weyrauch³⁰, N. Whitehorn²³, C. H. Wiebusch¹, D. R. Williams⁵⁸, L. Witthaus²², M. Wolf²⁶, G. Wrede²⁵, X. W. Xu⁵, J. P. Yañez²⁴, Y. Yao³⁹, E. Yildizci³⁹, S. Yoshida¹⁵, R. Young³⁵, F. Yu¹³, S. Yu⁵², T. Yuan³⁹, A. Zegarelli⁹, S. Zhang²³, Z. Zhang⁵⁵, P. Zhelnin¹³, P. Zilberman³⁹

¹ III. Physikalisches Institut, RWTH Aachen University, D-52056 Aachen, Germany

² Department of Physics, University of Adelaide, Adelaide, 5005, Australia

³ Dept. of Physics and Astronomy, University of Alaska Anchorage, 3211 Providence Dr., Anchorage, AK 99508, USA

⁴ School of Physics and Center for Relativistic Astrophysics, Georgia Institute of Technology, Atlanta, GA 30332, USA

⁵ Dept. of Physics, Southern University, Baton Rouge, LA 70813, USA

⁶ Dept. of Physics, University of California, Berkeley, CA 94720, USA

⁷ Lawrence Berkeley National Laboratory, Berkeley, CA 94720, USA

⁸ Institut für Physik, Humboldt-Universität zu Berlin, D-12489 Berlin, Germany

⁹ Fakultät für Physik & Astronomie, Ruhr-Universität Bochum, D-44780 Bochum, Germany

¹⁰ Université Libre de Bruxelles, Science Faculty CP230, B-1050 Brussels, Belgium

- ¹¹ Vrije Universiteit Brussel (VUB), Dienst ELEM, B-1050 Brussels, Belgium
- ¹² Dept. of Physics, Simon Fraser University, Burnaby, BC V5A 1S6, Canada
- ¹³ Department of Physics and Laboratory for Particle Physics and Cosmology, Harvard University, Cambridge, MA 02138, USA
- ¹⁴ Dept. of Physics, Massachusetts Institute of Technology, Cambridge, MA 02139, USA
- ¹⁵ Dept. of Physics and The International Center for Hadron Astrophysics, Chiba University, Chiba 263-8522, Japan
- ¹⁶ Department of Physics, Loyola University Chicago, Chicago, IL 60660, USA
- ¹⁷ Dept. of Physics and Astronomy, University of Canterbury, Private Bag 4800, Christchurch, New Zealand
- ¹⁸ Dept. of Physics, University of Maryland, College Park, MD 20742, USA
- ¹⁹ Dept. of Astronomy, Ohio State University, Columbus, OH 43210, USA
- ²⁰ Dept. of Physics and Center for Cosmology and Astro-Particle Physics, Ohio State University, Columbus, OH 43210, USA
- ²¹ Niels Bohr Institute, University of Copenhagen, DK-2100 Copenhagen, Denmark
- ²² Dept. of Physics, TU Dortmund University, D-44221 Dortmund, Germany
- ²³ Dept. of Physics and Astronomy, Michigan State University, East Lansing, MI 48824, USA
- ²⁴ Dept. of Physics, University of Alberta, Edmonton, Alberta, T6G 2E1, Canada
- ²⁵ Erlangen Centre for Astroparticle Physics, Friedrich-Alexander-Universität Erlangen-Nürnberg, D-91058 Erlangen, Germany
- ²⁶ Physik-department, Technische Universität München, D-85748 Garching, Germany
- ²⁷ Département de physique nucléaire et corpusculaire, Université de Genève, CH-1211 Genève, Switzerland
- ²⁸ Dept. of Physics and Astronomy, University of Gent, B-9000 Gent, Belgium
- ²⁹ Dept. of Physics and Astronomy, University of California, Irvine, CA 92697, USA
- ³⁰ Karlsruhe Institute of Technology, Institute for Astroparticle Physics, D-76021 Karlsruhe, Germany
- ³¹ Karlsruhe Institute of Technology, Institute of Experimental Particle Physics, D-76021 Karlsruhe, Germany
- ³² Dept. of Physics, Engineering Physics, and Astronomy, Queen's University, Kingston, ON K7L 3N6, Canada
- ³³ Department of Physics & Astronomy, University of Nevada, Las Vegas, NV 89154, USA
- ³⁴ Nevada Center for Astrophysics, University of Nevada, Las Vegas, NV 89154, USA
- ³⁵ Dept. of Physics and Astronomy, University of Kansas, Lawrence, KS 66045, USA
- ³⁶ Centre for Cosmology, Particle Physics and Phenomenology - CP3, Université catholique de Louvain, Louvain-la-Neuve, Belgium
- ³⁷ Department of Physics, Mercer University, Macon, GA 31207-0001, USA
- ³⁸ Dept. of Astronomy, University of Wisconsin—Madison, Madison, WI 53706, USA
- ³⁹ Dept. of Physics and Wisconsin IceCube Particle Astrophysics Center, University of Wisconsin—Madison, Madison, WI 53706, USA
- ⁴⁰ Institute of Physics, University of Mainz, Staudinger Weg 7, D-55099 Mainz, Germany
- ⁴¹ Department of Physics, Marquette University, Milwaukee, WI 53201, USA
- ⁴² Institut für Kernphysik, Universität Münster, D-48149 Münster, Germany
- ⁴³ Bartol Research Institute and Dept. of Physics and Astronomy, University of Delaware, Newark, DE 19716, USA
- ⁴⁴ Dept. of Physics, Yale University, New Haven, CT 06520, USA
- ⁴⁵ Columbia Astrophysics and Nevis Laboratories, Columbia University, New York, NY 10027, USA
- ⁴⁶ Dept. of Physics, University of Oxford, Parks Road, Oxford OX1 3PU, United Kingdom
- ⁴⁷ Dipartimento di Fisica e Astronomia Galileo Galilei, Università Degli Studi di Padova, I-35122 Padova PD, Italy
- ⁴⁸ Dept. of Physics, Drexel University, 3141 Chestnut Street, Philadelphia, PA 19104, USA
- ⁴⁹ Physics Department, South Dakota School of Mines and Technology, Rapid City, SD 57701, USA
- ⁵⁰ Dept. of Physics, University of Wisconsin, River Falls, WI 54022, USA
- ⁵¹ Dept. of Physics and Astronomy, University of Rochester, Rochester, NY 14627, USA
- ⁵² Department of Physics and Astronomy, University of Utah, Salt Lake City, UT 84112, USA
- ⁵³ Dept. of Physics, Chung-Ang University, Seoul 06974, Republic of Korea
- ⁵⁴ Oskar Klein Centre and Dept. of Physics, Stockholm University, SE-10691 Stockholm, Sweden
- ⁵⁵ Dept. of Physics and Astronomy, Stony Brook University, Stony Brook, NY 11794-3800, USA
- ⁵⁶ Dept. of Physics, Sungkyunkwan University, Suwon 16419, Republic of Korea
- ⁵⁷ Institute of Physics, Academia Sinica, Taipei, 11529, Taiwan
- ⁵⁸ Dept. of Physics and Astronomy, University of Alabama, Tuscaloosa, AL 35487, USA
- ⁵⁹ Dept. of Astronomy and Astrophysics, Pennsylvania State University, University Park, PA 16802, USA
- ⁶⁰ Dept. of Physics, Pennsylvania State University, University Park, PA 16802, USA
- ⁶¹ Dept. of Physics and Astronomy, Uppsala University, Box 516, SE-75120 Uppsala, Sweden
- ⁶² Dept. of Physics, University of Wuppertal, D-42119 Wuppertal, Germany
- ⁶³ Deutsches Elektronen-Synchrotron DESY, Platanenallee 6, D-15738 Zeuthen, Germany
- ^a also at Institute of Physics, Sachivalaya Marg, Sainik School Post, Bhubaneswar 751005, India
- ^b also at Department of Space, Earth and Environment, Chalmers University of Technology, 412 96 Gothenburg, Sweden
- ^c also at INFN Padova, I-35131 Padova, Italy
- ^d also at Earthquake Research Institute, University of Tokyo, Bunkyo, Tokyo 113-0032, Japan
- ^e now at INFN Padova, I-35131 Padova, Italy

Acknowledgments

The authors gratefully acknowledge the support from the following agencies and institutions: USA – U.S. National Science Foundation-Office of Polar Programs, U.S. National Science Foundation-Physics Division, U.S. National Science Foundation-EPSCoR, U.S. National Science Foundation-Office of Advanced Cyberinfrastructure, Wisconsin Alumni Research Foundation, Center for High Throughput Computing (CHTC) at the University of Wisconsin–Madison, Open Science Grid (OSG), Partnership to Advance Throughput Computing (PATH), Advanced Cyberinfrastructure Coordination Ecosystem: Services & Support (ACCESS), Frontera and Ranch computing project at the Texas Advanced Computing Center, U.S. Department of Energy-National Energy Research Scientific Computing Center, Particle astrophysics research computing center at the University of Maryland, Institute for Cyber-Enabled Research at Michigan State University, Astroparticle physics computational facility at Marquette University, NVIDIA Corporation, and Google Cloud Platform; Belgium – Funds for Scientific Research (FRS-FNRS and FWO), FWO Odysseus and Big Science programmes, and Belgian Federal Science Policy Office (Belspo); Germany – Bundesministerium für Forschung, Technologie und Raumfahrt (BMFTR), Deutsche Forschungsgemeinschaft (DFG), Helmholtz Alliance for Astroparticle Physics (HAP), Initiative and Networking Fund of the Helmholtz Association, Deutsches Elektronen Synchrotron (DESY), and High Performance Computing cluster of the RWTH Aachen; Sweden – Swedish Research Council, Swedish Polar Research Secretariat, Swedish National Infrastructure for Computing (SNIC), and Knut and Alice Wallenberg Foundation; European Union – EGI Advanced Computing for research; Australia – Australian Research Council; Canada – Natural Sciences and Engineering Research Council of Canada, Calcul Québec, Compute Ontario, Canada Foundation for Innovation, WestGrid, and Digital Research Alliance of Canada; Denmark – Villum Fonden, Carlsberg Foundation, and European Commission; New Zealand – Marsden Fund; Japan – Japan Society for Promotion of Science (JSPS) and Institute for Global Prominent Research (IGPR) of Chiba University; Korea – National Research Foundation of Korea (NRF); Switzerland – Swiss National Science Foundation (SNSF).